Physical modelling of tidal stream turbine wake structures under yaw conditions

energies

MDPI

Article

Physical Modelling of Tidal Stream Turbine Wake Structures under Yaw Conditions

Can Zhang [1,2], Jisheng Zhang [1,*], Athanasios Angeloudis [3], Yudi Zhou [1], Stephan C. Kramer [2] and Matthew D. Piggott [2,*]

[1] College of Harbor, Coastal and Offshore Engineering, Hohai University, Nanjing 210098, China
[2] Department of Earth Science and Engineering, Imperial College London, London SW7 2AZ, UK
[3] School of Engineering, Institute for Infrastructure and the Environment, The University of Edinburgh, Edinburgh EH8 9JU, UK
* Correspondence: jszhang@hhu.edu.cn (J.Z.); m.d.piggott@imperial.ac.uk (M.D.P.)

Abstract: Tidal stream turbines may operate under yawed conditions due to variability in ocean current directions. Insight into the wake structure of yawed turbines can be essential to ensure efficient tidal stream energy extraction, especially for turbine arrays where wake interactions emerge. We studied experimentally the effects of turbines operating under varying yaw conditions. Two scenarios, including a single turbine and a set of two turbines in alignment, were configured and compared. The turbine thrust force results confirmed that an increasing yaw angle results in a decrease in the turbine streamwise force and an increase in the turbine spanwise force. The velocity distribution from the single turbine scenario showed that the wake deflection and velocity deficit recovery rate increased at a rate proportional to the yaw angle. The two-turbine scenario results indicated that the deployment of an upstream non-yawed turbine significantly limited the downstream wake steering (i.e., the wake area behind the downstream turbine). Interestingly, a yawed downstream turbine was seen to influence the steering of both the upstream and the downstream wakes. These systematically derived data could be regarded as useful references for the numerical modelling and optimisation of large arrays.

Keywords: tidal stream energy; experiment; wake structure; yaw angles; turbine alignment

Citation: Zhang, C.; Zhang, J.; Angeloudis, A.; Zhou, Y.; Kramer, S.C.; Piggott, M.D. Physical Modelling of Tidal Stream Turbine Wake Structures under Yaw Conditions. *Energies* **2023**, *16*, 1742. https://doi.org/10.3390/en16041742

Academic Editor: Saeed Badshah

Received: 15 January 2023
Revised: 4 February 2023
Accepted: 7 February 2023
Published: 9 February 2023

1. Introduction

Tidal stream energy represents an attractive renewable energy source because of its predictability [1]. Kinetic energy stored within high-magnitude tidal stream currents can be converted into electricity through tidal energy converters [2,3]. In energetic sites, the prevailing power generation strategy will likely involve the concentration of turbines in an array to harness tidal stream energy in the most-efficient manner possible [4]. However, due to non-rectilinear directional changes over the ebb and flood tides alongside higher-frequency flow variations that include those induced by inter-array turbine interactions, devices in an array can often operate under yaw conditions [5]; this can be either intentional for wake steering purposes or a result of flow misalignment [6]. As the yawed turbine's rotor plane is not perpendicular to the incoming flow, a horizontal axis turbine's performance degrades, while its wake flow undergoes a deflection or "steering" [7]. Investigating the wake structure of yawed turbines is an important task, especially in the context of the contribution this phenomenon may be able to make to maximise an array's total energy output, as well as being a source of array yield uncertainty.

Wake steering is a concept that is widely appreciated in wind farms [8]. If an upwind wind turbine has the capacity to control its yaw angle, its resulting wake can be steered away from downwind turbines. In doing so, the whole array could be deployed in a compact layout, aiding spatial planning and improving overall array performance [9,10]. In order to understand the potential of wake steering and to exploit it effectively, studies have

so far explored the effects of yaw angle on wind turbine performance. By applying physical experiments, Bastankhah and Porté-Agel observed turbine performance degradation and a turbine thrust force reduction as the yaw angle increases [11]. Similarly, Gao et al. [12] developed an actuator line model with large-eddy simulation introducing a new anisotropic body-force projection model to study the effect of the nacelle on the wind turbine wake. They found that nacelle effects can significantly affect wind turbine wakes, especially under yaw conditions. Moreover, Dijk et al. [13] observed that overall power production can increase when upwind turbines yaw, and loading on downwind turbines drops in cases of partial wake overlap evasion. Similar conclusions on turbine performance and thrust force have been reported in other studies [10,14,15]. For two aligned wind turbines [9], it was found that the spacing between turbines and the yaw angle of the upwind turbine plays a significant role in the overall wind farm efficiency. Specifically, the results confirmed that, by operating an upwind turbine under appropriate yaw conditions, wind farm performance can be comparable to a more conservative separation distance of turbines that would otherwise be fixed at zero yaw angles. For wind farms with multi-row turbine arrangements, Bastankhah and Porté-Agel [16] confirmed that turbine yawing provides a route to boost overall performance. Their results showed that the maximum total power enhancement could reach 17% when compared to a fully non-yawed case. The optimal distribution of yaw angles followed a decreasing trend in the yaw angle value from the upwind to the downwind turbines.

Few studies have concentrated on the performance of horizontal axis tidal stream turbines under yawed conditions. Partly, wake steering in tidal turbines could be perceived to be of secondary importance given that the tidal flow direction is more predictable. However, hotspots in tidal stream resources tend to emerge in confined areas, leading to incentives to pack turbines closer together, which would make wake steering more important and potentially more valuable. Similar to wind turbines, physical experiments to-date indicate that yawed tidal stream turbines experience reduced thrust force and power extraction [17,18]. Results from numerical models also confirmed that, as the yaw angle increases, power generation and axis thrust reduce [19,20]. Baratchi et al. [21] simulated yawed turbine behaviour using the actuator line method, and their numerical results showed good agreement with the measurements published in [17]. Wang et al. [22] simulated a yawed turbine using the $k-\omega$ SST turbulence model from the ANSYS Fluent CFD package. Their numerical model was validated against experimental data, confirming that the axial force coefficient and the power coefficient were reduced for the yawed turbine. They also found that the asymmetry of the wake velocity distribution became more apparent with increasing yaw angle. Modali et al. [7] studied turbine performance and wake deflection within $\pm 15^{\circ}$ yawed conditions. Their results showed a $\approx$10% reduction in the maximum power coefficient. They also found that when the upstream turbine is yawed, the downstream turbine can extract more than 50% higher energy in a staggered layout than in an aligned layout. Interestingly, Borg et al. [23] investigated the performance of a ducted tidal turbine under yaw conditions and found that, with the inclusion of a duct, the resultant axial force loading on the blades was enhanced, sustaining the performance of the yawed turbine.

Previous physical modelling experiments of yawed tidal stream turbines focused on power and the thrust force coefficient variations as the yaw angle changes. However, there are limited wake velocity data from yawed tidal stream turbines, which represents a significant hindrance to the validation of theoretical and numerical models. We seek to address this herein. To the best of our knowledge, there has been little work reported on the influence of upstream or downstream turbines on wake evolution. This would be a common scenario when considering yaw angle control across a tidal stream turbine array. It would also be a vital component to inform the optimisation of tidal stream turbine array design [4,24,25]. Therefore, we experiment with yawed turbine configurations, covering both single-turbine and two-turbine scenarios. The latter is intentionally positioned in an aligned configuration. Turbine thrust force and wake velocity distributions were measured

in all cases considered. The objective of the single-turbine scenario was to investigate the wake structure at hub height for the turbine under a range of yaw conditions and examine how the wake area changes with an increase in the yaw angle. In turn, the single-turbine case acts as a baseline for the two-turbine scenario, where the velocity distribution changes caused by the existence of an upstream or downstream turbine were studied.

2. Experimental Setup

2.1. Flow Flume and the Measurement Device

Experiments were conducted in a recirculating flow flume designed and constructed at Hohai University, as shown in Figure 1, with further details given in Zhou et al. [26]. The flume is 50 m long, 5 m wide, and 0.7 m deep. The incoming flow velocity was driven by pumps located upstream, together with baffles at the downstream end that regulate the flow depth and exit velocity. These features allow a constant inflow velocity and stable water depth to be achieved. In order to dissipate large-scale flow structures such as eddies and straighten the flow, two screens of variable porosity are inserted at the inlet of the flume.

Figure 1. Experimental setup at the circulating flow flume. The left picture shows the movable platform on which the Nortek Vectrino Profiler is positioned. The right picture shows the porous walls at the inlet of the flume.

Flow velocity downstream of turbine wakes was measured using a downward-facing Nortek Vectrino Profiler, shown in Figure 2a. The sampling frequency of the device was set at 100 Hz, monitoring a cylindrical volume at 40 mm below the probe of 6 mm diameter and extending a depth of 30 mm and, hence, here extending all the way to the bottom of the flume. The measurement accuracy of the device is $\pm 0.5\%$. To ensure the reliability of the measured velocity, the manufacturer recommended that the signal-to-noise ratio (SNR) should be maintained at a level higher than 15 dB and the correlation of the data used for the analysis should be in the order of 80% at least during the data collection. The Nortek Vectrino Profiler was positioned on a movable platform, which ensured accurate positioning for velocity sampling.

An ATI-gamma six-axis force–torque sensor was used to measure the force induced by the flow on the turbine, as in Figure 2b. The sensor can measure the thrust force and the torque at the same time. The measurement accuracy of the device is $\pm 0.3\%$. The maximum measurable values of the sensor are 65 N and 5 $N \cdot m$ for thrust force and the torque respectively. The sensor has a frequency of 100 Hz, and its accuracy is within 0.3%.

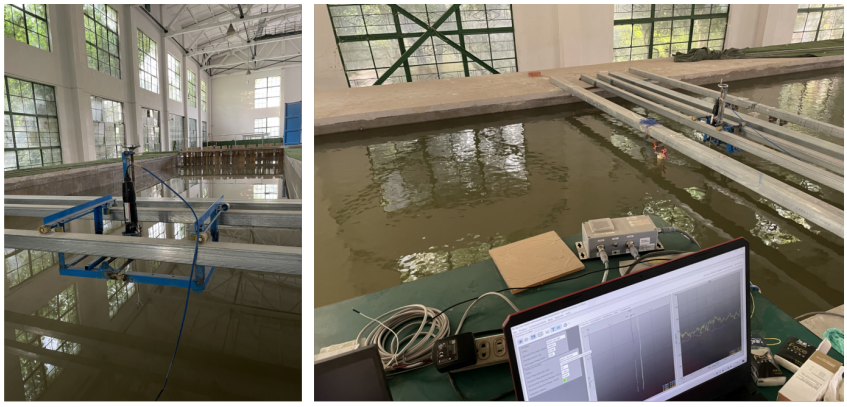

(**a**)

(**b**)

Figure 2. The measurement devices, as positioned in the flume at Hohai University. (**a**) The downward-facing Nortek Vectrino Profiler is positioned on a movable platform. (**b**) The ATI-gamma six-axis force–torque sensor.

2.2. Turbine Physical Model

The turbine models comprise two 3-bladed rotors (Figure 3), manufactured using 3D printing with UV curable resin. The airfoil of the blades was taken to be NREL-S822, as per Wang [27]. The two turbines have the same diameter $D = 0.3$ m and a cylindrical support structure diameter of 0.06 m, which is offset from the rotor plane by 0.08 m. The turbine hub height above the flume floor is 0.25 m. As the water depth was set to $H = 0.5$ m, the minimum distances from the blade tip to the flume floor and the water surface were both 0.1 m during the operation. This corresponds to a distance of $0.2H$ between the sea bed and the bottom of the rotor, which is similar to the constraints expected in practice ($\approx 0.25H$ [28]) to avoid the rotor being positioned in the lowest region of the water column. Considering the reduced surface roughness of a concrete-lined channel, we considered this sufficient. In addition, the $0.2H$ clearance from the top of the rotor to the sea surface was aligned with the expected clearance constraints (typically, these are in the order of 8 m for a device located at a 35–40 m depth), rendering the physical model consistent with the boundary effects experienced in practice. The same setup can be found in [29].

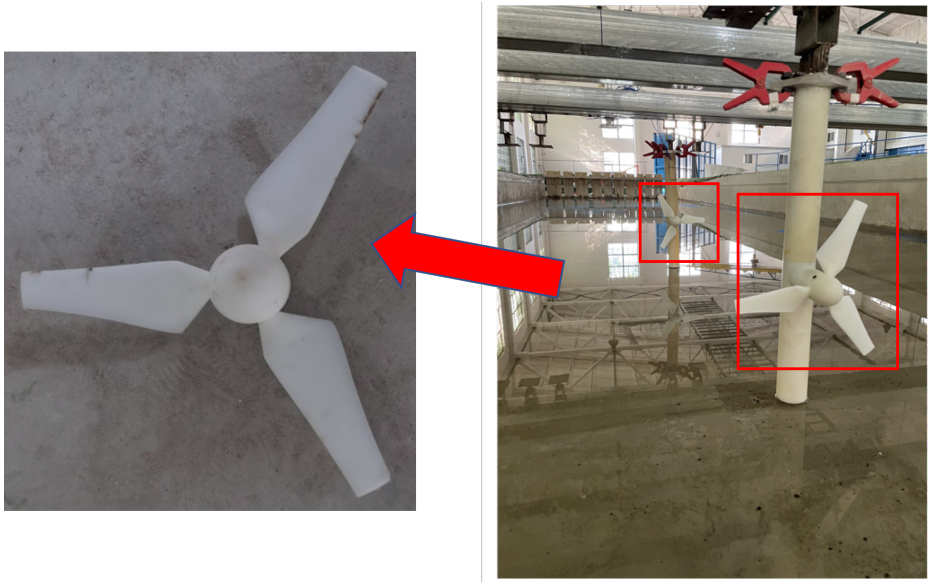

Figure 3. The physical model of the turbine deployed in the experiments.

2.3. Case Studies

In investigating the wake structure and the interactions between yawed turbines, 11 case studies of varying yaw conditions were considered. The range of the yaw angles γ followed from the literature. Indicatively, Bartl et al. [14] studied wind turbine performance by varying γ from 0° to 40°, while Galloway et al. [18] investigated tidal stream turbine performance for γ from 0° to 22.5°. As the tidal flow direction is more predictable, we opted to focus here on a γ range of 0°–30°.

The cases can be further classified into two configurations:

Scenario 1 Yaw of a single turbine from 0° to 30°.

Scenario 2 Yaw of one of two turbines from 0° to 30° while retaining the other turbine in a non-yawed state relative to the flume. The distance between the turbines was fixed at 5D (see Figure 4b).

More details are summarised in Table 1. The case including both turbines at $\gamma = 0°$ was treated as the baseline for Scenario 2.

Table 1. The yaw angle values considered for each experiment case.

Scenarios	Case ID	Yaw Angle γ (°)	
		Upstream Turbine	Downstream Turbine
Scenario 1	1	0	–
	2	10	–
	3	20	–
	4	30	–
Scenario 2	5	0	30
	6	0	20
	7	0	10
	8	0	0
	9	10	0
	10	20	0
	11	30	0

For the fixed water depth of $H = 0.5$ m, the average inflow velocity u_0 was set to 0.33 m/s, which equates to a Froude number of $Fr = 0.15$. This value corresponds to typical operational conditions, i.e., at a depth of 40 m and a ≈ 3.0 m/s streamwise flow magnitude. The width of the flume is $L_w = 5$ m, so the blockage ratio can be calculated

as $a = \pi \times (D/2)^2/(L_w \times H) = \pi \times (0.6/2)^2/(5 \times 0.5) \approx 2.8\%$, which is much smaller compared to previous experimental studies, such as 8.7% in Zang et al. [30] and 16.4% in Chen et al. [31]. By retaining the blockage ratio at such a low value, we expect blockage effects to be consistent with real deployment scenarios. We focused on the horizontal velocity plane at hub height where steering effects would be pronounced, in alignment with related studies on wake recovery measurements [11,26,32].

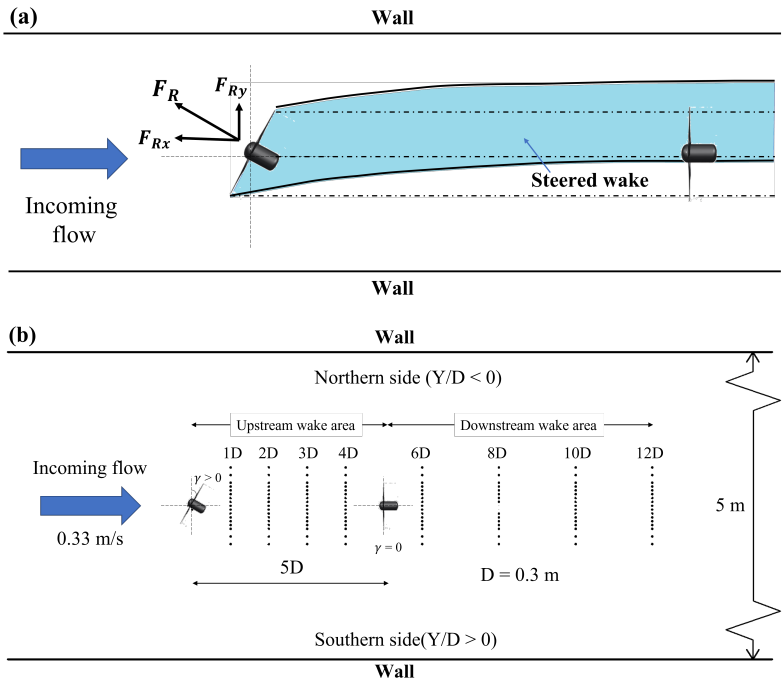

Figure 4. (**a**) Schematic of the yawed turbine thrust force and the assumed wake steering; (**b**) turbine deployments and structure of the sampling grids and the definition of the yaw angle value γ.

For Scenario 1, we used the Nortek Vectrino Profiler to measure the flow velocities across six cross-sections of the turbine's wake area at $1D$, $2D$, $3D$, $4D$, $6D$, and $8D$ downstream. In turn, Scenario 2 follows the setup of Bastankhah and Porté-Agel [11]. In Scenario 2, velocity measurements were carried out over eight cross-sections; the measurement areas were set at $1D$, $2D$, $3D$, $4D$, $6D$, $8D$, $10D$, and $12D$ downstream. The spanwise sampling points commenced at $Y = -1D$ and ended at $Y = 1D$ to capture the steered wake, as in Figure 4a. A similar approach can be seen in [33,34]. The whole layout of the measurement sampling points is sketched in Figure 4b. The rotor orientation was tested in 10° increments from 0° to 30°. We define the yaw angles as zero when the rotor is perpendicular to the velocity at the inflow flume boundary. A clockwise rotation corresponds to a positive angle, i.e., $\gamma > 0^\circ$, as shown in Figure 4b.

During the velocity measurement, the SNR value was maintained above 20 dB, and the correlation remained above 90%; higher than the manufacturer-recommended minimum values of 15 dB and 80%, respectively, contributing to the reliability of the Nortek Vectrino Profiler sampling. Zhang et al. [29] previously used the same force–torque sensing approach in their study, where they found that the deviation of the mean value of thrust force obtained from a 180 s sampling duration was within a range of 0.35% relative to that obtained by a 600 s sampling duration. This deviation was deemed acceptable. Increasing the sampling time from 180 s to 360 s only led to an 0.11% deviation improvement. The sampling duration for turbine thrust in their study was taken as 300 s. We imposed the same sampling duration of 300 s to ensure an equivalent level of data accuracy balancing experimentation time constraints.

2.4. Experimental Data Analysis

As wave conditions were not considered in this study, instantaneous velocity can be split into a mean velocity $\overline{u_i}$ and a fluctuating velocity $u_i^{'}$, where i is the index of the samples.

$$u_i = \overline{u} + u_i^{'}. \tag{1}$$

The phase-averaged method was applied to process the measured data. The averaged streamwise velocity $\overline{u}$ is defined as

$$\overline{u} = \frac{1}{N}\sum_{i=1}^{N} u_i, \tag{2}$$

where N is the number of samples taken during the measurement. The magnitude of the velocity at the measurement point is calculated as

$$|\overline{u}| = \sqrt{\overline{u_x}^2 + \overline{u_y}^2 + \overline{u_z}^2}. \tag{3}$$

In order to investigate velocity deficit and flow recovery, relevant parameters were normalised by the inflow velocity magnitude $|u_0|$. The relative value of the normalised velocity is $|u/u_0|$, and for simplicity, we refer to it as u/u_0 in the following sections. Streamwise turbulence intensity was also captured and is defined as

$$TI_x = \frac{\sqrt{\overline{u_x'^2}}}{u_0} \times 100\%. \tag{4}$$

As per the wind energy literature [35,36], yawed turbine wakes usually show clear asymmetric characteristics in the spanwise direction. Therefore, it is necessary to track the wake centreline to evaluate differences in varying yaw angles [37]. There are several approaches proposed in wind studies to capture the wake centreline, such as fitting a Gaussian shape [35,38], using the "Centre of Mass" of the velocity deficit [7,39,40], or tracking the wake centreline using particle tracking [41]. In this study, the "Centre of Mass" method was applied. For each downstream cross-section, coordinates at the centre of the wake $y_c(x)$ can be calculated as

$$y_c = \frac{\int y\Delta u(x,y)\,\mathrm{dy}}{\int \Delta u(x,y)\,\mathrm{dy}}, \tag{5}$$

where $\Delta u(x,y)$ is the velocity deficit, defined as $1 - |u(x,y)/u_0|$, where $u(x,y)$ is the measured velocity at location (x,y). As the velocity measurements taken along the spanwise direction are discrete, the integrals were replaced by the weighted sum of the discrete data.

As the ATI-gamma six-axis force–torque sensor is only able to measure the thrust force on the whole structure, the total force F can be decomposed into the support structure force F_s and the turbine rotor force F_R, respectively. The support structure force F_S was obtained in a separate experiment without the turbine rotor and measuring the total force in that situation. Then, the turbine rotor force can be calculated as

$$F_R = F - F_S. \tag{6}$$

It should be noted that this approach assumes that the thrust force of the structure is not influenced by the presence of the rotor.

3. Results and Discussion

3.1. Thrust Force

Figure 5a shows the yawed turbine thrust forces F_R obtained by subtracting the measured support force F_S from the total measured force F. Streamwise force F_{Rx} decreases with

increments of γ, as expected. For the single-turbine (Scenario 1) and the upstream turbine (Scenario 2) cases, the force reductions were similar: both dropped by $\approx 12\%$ when $\gamma = 30^\circ$ compared to the non-yawed cases. The reduction level was consistent with the results from Modali et al. [42], where an 8% thrust force decline was observed when $\gamma = 15^\circ$. The similarity between the single-turbine and yawed upstream turbine case confirmed that the downstream non-yawed turbine had a negligible effect on the performance of the upstream turbine. There was an outlier value when the upstream turbine $\gamma = 10^\circ$, likely due to a sensor malfunction, which is plotted in Figure 5a for completeness, but was otherwise excluded in the analysis.

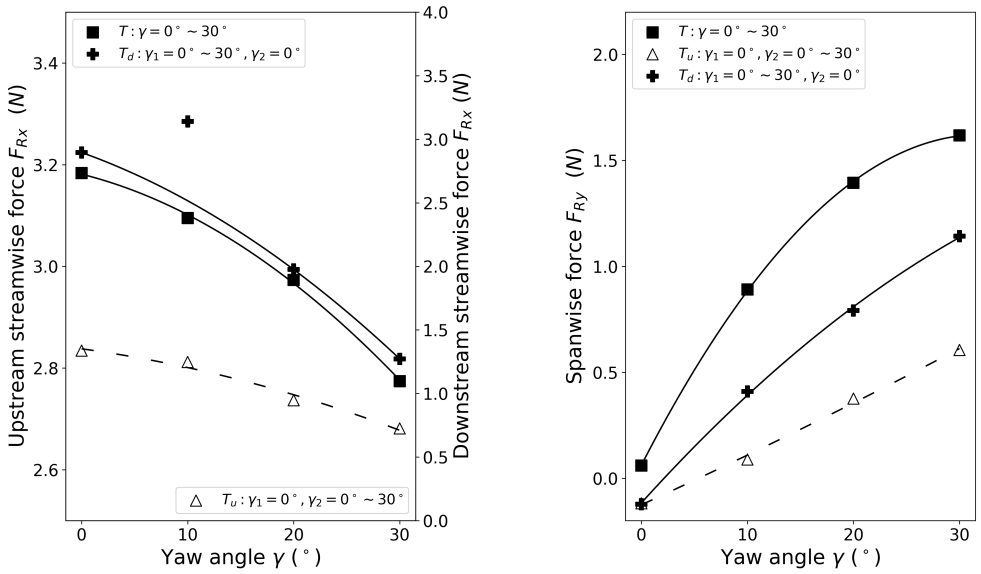

(**a**)

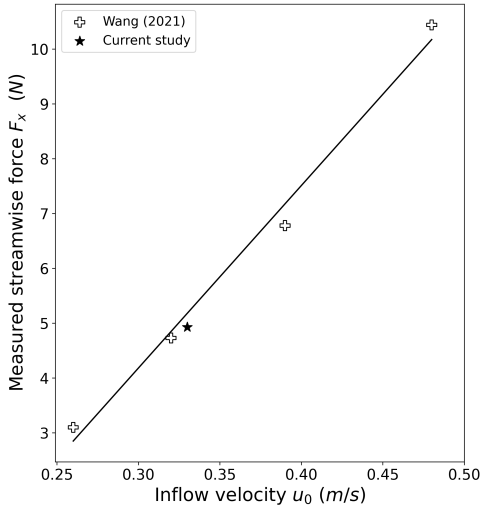

(**b**)

Figure 5. Thrust forces recorded.T: Turbine of Scenario 1; T_u: Upstream turbine of Scenario 2; T_d: Downstream turbine of Scenario 2. (**a**) Variation of thrust force vs yaw angle γ. (**b**) Validation of the non-yawed turbine's whole thrust force in Scenario 1 alongside data of Wang [27].

For the downstream yawed turbine cases, the thrust force was lesser as it was deployed in the wake of the upstream turbine and was, thus, subjected to a reduced streamwise velocity. For $\gamma = 0^\circ - 30^\circ$, the thrust force saw a significant reduction in the downstream turbine streamwise force, measured at 46%. This might be due to the decreased inflow velocity caused by the upstream turbine and its effect downstream.

The right-hand plot of Figure 5a shows the variation of the turbine spanwise force F_{Ry}. For $\gamma = 0°$, the spanwise force was nearly zero. With $\gamma > 0°$, the spanwise force increased, leading to the wake steering, as discussed in the next section.

Separately, the measured F for a non-yawed turbine was measured at 4.93 N, when $u_0 = 0.33\ m/s$. The data from Wang [27] on the thrust force variation with increasing inflow velocity are plotted in Figure 5b alongside our data, suggesting a consistent behaviour with the literature.

3.2. Wake Velocity Distribution

3.2.1. Scenario 1: Single Turbine

Figure 6a presents the normalised velocity u/u_0 distribution in the turbine wake area under different yaw conditions. For $\gamma = 0°$, the wake was largely symmetric downstream from $1D$ to $8D$ as the wake propagation was aligned with the free-stream flow. For $\gamma > 0°$, apparent wake steering emerged, leading to an asymmetric velocity distribution. The asymmetry increased with γ. As the turbine yawed clockwise, its wake area is tilted to the "northern" side of the flume, leading to a more significant velocity deficit there than for the "southern" side.

In the near-wake area ($X/D \leq 4$), the velocity deficits for all cases had a similar magnitude on the northern side ($Y/D > 0$), while apparent differences occurred on the southern side ($Y/D \leq 0$). Across cases, the significant velocity deficit regions coincided, decreasing by 65% at a $1D$ downstream compared to the inflow velocity u_0. For $\gamma = 0°$, the velocity recovered to 41.27% of u_0 at a distance of $4D$ downstream, while the yawed turbines had a higher recovery rate by this distance. For $\gamma = 30°$ in particular, the lowest velocity reached 60% of the inflow velocity at a $4D$ downstream, which was 18.7% higher than for $\gamma = 0°$. In other words, as the yawed turbine extracted less energy from the flow, it had a lower effect on the wake area. As such, the deficit values in the wakes of the yawed turbines had smaller magnitudes than in the non-yawed case.

Figure 6b shows the contour plots of the velocity distribution and the relative plots by subtracting the normalised results of the $\gamma = 0°$ baseline from the $\gamma > 0°$ cases. It can be seen that the value of $\Delta u/u_0 = (u_{\gamma=i} - u_{\gamma=0°})/u_0$, for $i \in [10°, 20°, 30°]$, was positive on the southern side and negative on the northern side. It can be explained as follows: as in Figure 4a, the y-component of the thrust force increased for $\gamma > 0°$, steering the wake towards the northern side, leading to mixing between the undisturbed bypass flow and the wake flow. Therefore, the bypass flow at the northern side decelerated and exhibited a similar wake velocity distribution to the non-yawed case. As for the southern side bypass flow, because the wake area was diverted northwards, much of the wake effects were avoided. As a result, $\Delta u/u_0$ remained at a high value in the near-wake area.

In the far-wake area ($X/D > 4$), the velocity recovery rate remained lower than 50% for $\gamma = 0°$ at a $5D$ downstream distance, while for the cases under yawed conditions, the velocity recovered to 60% of u_0 by that cross-section. As the flow propagated further downstream, the recovery rate for all cases decelerated. Finally, at $8D$ downstream, the wake areas shared a similar profile, in that the velocity converged to 70% of the inflow velocity in the central wake region, while the velocity recovery of 80% was reached at both the southern and northern sides. However, wake steering was still apparent in the far-wake area. Indicatively, the lowest velocity for $\gamma = 30°$ at $X/D = 8.0$ occurred at $Y/D = 0.25$, demonstrating the impact of wake steering. The contour plot of the far wake area showed that the difference between the non-yawed and yawed cases was less significant (see Figure 6b). $\Delta u/u_0$ dropped to 0.20 and then kept decreasing as observed at an $8D$ downstream. This was because the wake flow was redirected to the northern side. The remaining difference in the far wake area was because: (1) an $8D$ was not sufficient for the wake to recover fully; (2) a yawed turbine led to wake steering, whereby the minimum velocity location being case-dependent.

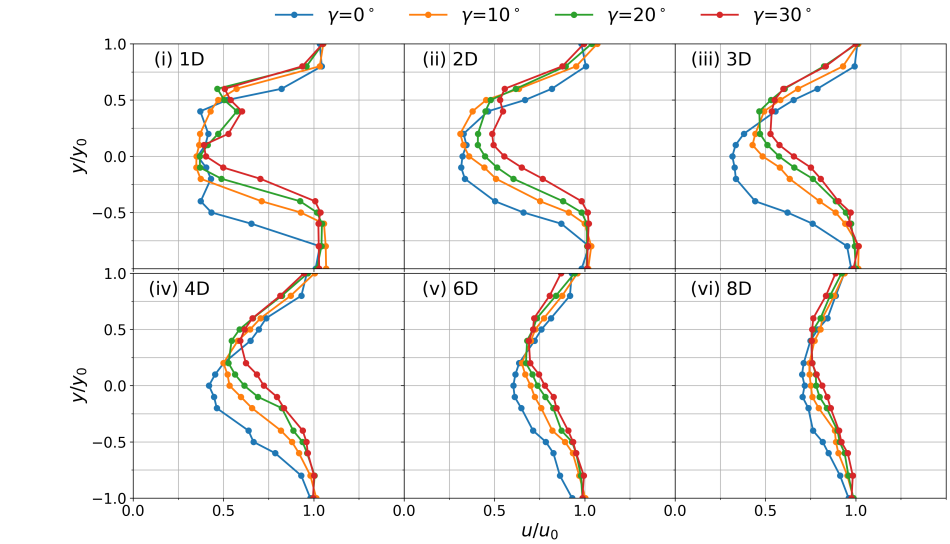

(**a**)

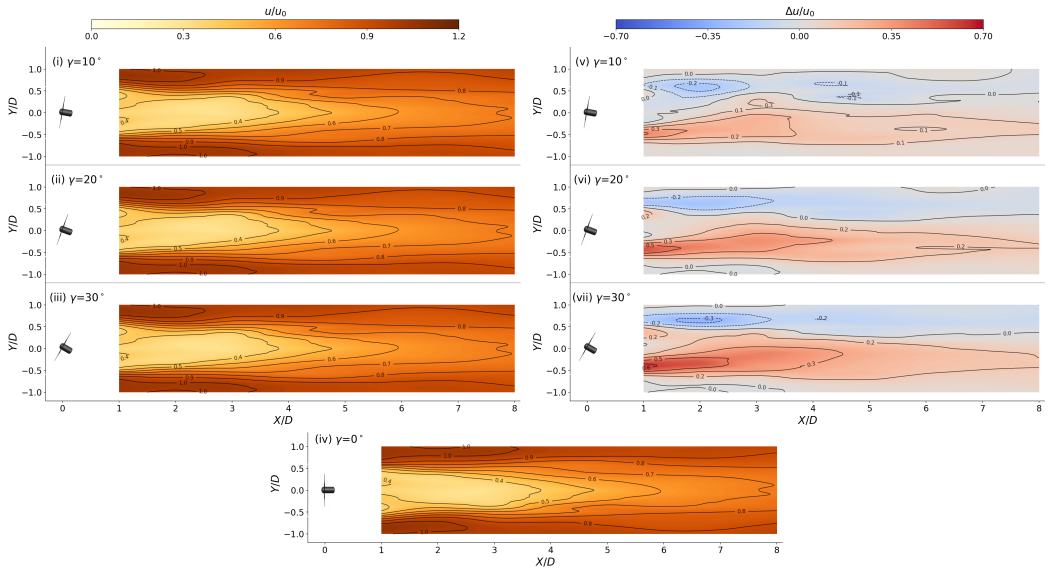

(**b**)

Figure 6. Wake velocity profiles for Scenario 1. (**a**) Normalised velocity distribution for the four cases of Scenario 1 at six downstream cross-sections. The separation distance between the profiles and the turbine are (i) $1D$, (ii) $2D$, (iii) $3D$, (iv) $4D$, (v) $6D$, and (vi) $8D$, respectively. (**b**) Normalised turbine wake velocity distributions for the cases of Scenario 1 and relative differences in normalised velocity between yawed and non-yawed turbine configurations: (i) $u/u_0 = u_{\gamma=10^\circ}/u_0$, (ii) $u/u_0 = u_{\gamma=20^\circ}/u_0$, (iii) $u/u_0 = u_{\gamma=30^\circ}/u_0$, (iv) $u/u_0 = u_{\gamma=0^\circ}/u_0$, (v) $\Delta u/u_0 = (u_{\gamma=10^\circ} - u_{\gamma=0^\circ})/u_0$, (vi) $\Delta u/u_0 = (u_{\gamma=20^\circ} - u_{\gamma=0^\circ})/u_0$, and (vii) $\Delta u/u_0 = (u_{\gamma=30^\circ} - u_{\gamma=0^\circ})/u_0$.

3.2.2. Scenario 2: Yawing One of the Two Turbines

In Scenario 2, we consider the two turbines deployed and separated by a $5D$ streamwise distance. In order to present the wake characteristics clearly, we refer to the region between the turbines as the "upstream wake area" (from $1D$ to $4D$ downstream of the first device) and the region downstream the second turbine as the "downstream wake area" (from $6D$ to $12D$).

It can be seen in Figures 7a and 8(i–iii) that varying the downstream turbine's yaw angle (γ_2) can affect the upstream wake area. As shown in Figure 7a(i–iv), at a $1D$, the velocity profiles for all cases were similar. However, as the flow propagated downstream, with $\gamma_2 > 0$, the distribution became asymmetric in the cross-stream direction. At $X/D = 4D$, wake recovery for the $\gamma_2 = 0^\circ$ was lower than the yawed cases when $\gamma_d = 10^\circ$ and 20°. It is conjectured that the $\gamma_2 = 0^\circ$ case provides the whole rotor-swept area as an obstacle that interferes with the flow, while the yawed turbines have smaller rotor-swept areas projected to the streamwise flow. Thus, the yawed turbines interacted with the flow less given that it is the projection of the turbine to the cross-stream direction that played a dominant role on the thrust forcing. However, the $\gamma_2 = 30^\circ$ case recorded this section's most-significant velocity deficit, especially for the southern side. Figure 7a(v–viii) presents the velocity distribution in the downstream wake area. In all cases, the velocities had similar magnitudes on the southern side at $X/D = 6.0$ (which was also at a $1D$ downstream from the downstream turbine). However, the velocity deficit was greater on the northern side when $\gamma_2 > 0$ due to wake steering.

Figure 8(viii—x) shows the relative plots between $\gamma_2 = 0$ and cases where $\gamma_2 > 0$. In the upstream wake area, as $\gamma_2 = 10^\circ$, velocity regions with $\Delta u/u_0 > 0$ appeared, which may be attributed to the downstream turbine strengthening the mixing effects, thus promoting upstream wake recovery. With $\gamma_2 > 10^\circ$, $\Delta u/u_0 > 0.1$ regions were suppressed. The lowest $\Delta u/u_0$ value was less than -0.2 when $\gamma_2 = 10^\circ$. For $\gamma_2 = 30^\circ$, the velocity in the upstream wake area decreased more compared to the non-yawed cases. The lowest $\Delta u/u_0$ under this condition was even smaller than -0.3. This may be because, when the downstream turbine operates under high values of γ_2, the rotation of the blades severely disturbs the flow in the upstream wake area. Across cases, the velocity deficit at a $6D$ downstream was most pronounced due to wake superposition. Compared to the $\gamma_2 = 0^\circ$ case, we can see that the $\gamma_2 > 0^\circ$ turbine cases had regions of $\Delta u/u_0 > 0$ that emerged at the southern side, while velocity deficit regions moved northwards due to wake steering. As $\gamma_2 = 20^\circ$, areas where the absolute value of $\Delta u/u_0 \approx 0.1$ at $\gamma_2 = 10^\circ$ expanded, with the changes exceeding $\Delta u/u_0$ of 0.2 due to greater wake steering effects. The wake area became significantly asymmetric when $\gamma_2 = 30^\circ$, with $\Delta u/u_0 < -0.2$. Meanwhile, the flow velocity to the southern side for this case was much faster than in the non-yawed cases, and $\Delta u/u_0 > 0.2$.

In Figures 7b and 8(iv–vi), the wake velocity profiles and contour plots are shown in the case where $\gamma_1 > 0$. As in Figure 7b(i–iv), wakes from $1D$ to $4D$ show a similar trend to that exhibited in Scenario 1. With increasing γ_1, the wake effects moved from the southern side northwards. As flow propagated further downstream, the velocity on the southern side recovered faster. At a $4D$ downstream, the velocity deficits had a closer agreement than in Scenario 1. This difference was due to the presence of the downstream turbine, which clearly affected the velocity profile upstream. Therefore, the downstream turbine dominated the velocity deficit, so that the difference among the four cases became much less. However, we hypothesised that this phenomenon could be attributed to scaling effects. As mentioned in Section 2.3, our experiment designed followed the Froude similarity with a full-scale realistic sea condition. As a result, the Reynolds number $Re = u_0 D/\nu$ of flow in the flume was $Re \approx 0.33 \times 0.3/10^{-6}$ = 99,000, which was orders of magnitude smaller than the value expected in a realistic condition. For reference, this would indicatively be in the order of $Re \approx 3 \times 40/10^{-6}$ = 120,000,000. Therefore, viscous forces had an unreasonably greater effect on the flow in the laboratory compared to what would be expected in practice. Figure 7b(v–viii) shows that downstream wakes steered in a similar level for all cases. This again confirmed that the downstream turbine can significantly limit the wake steering caused by the yawed upstream turbine, which may again be because of the smaller Reynolds number compared to realistic conditions.

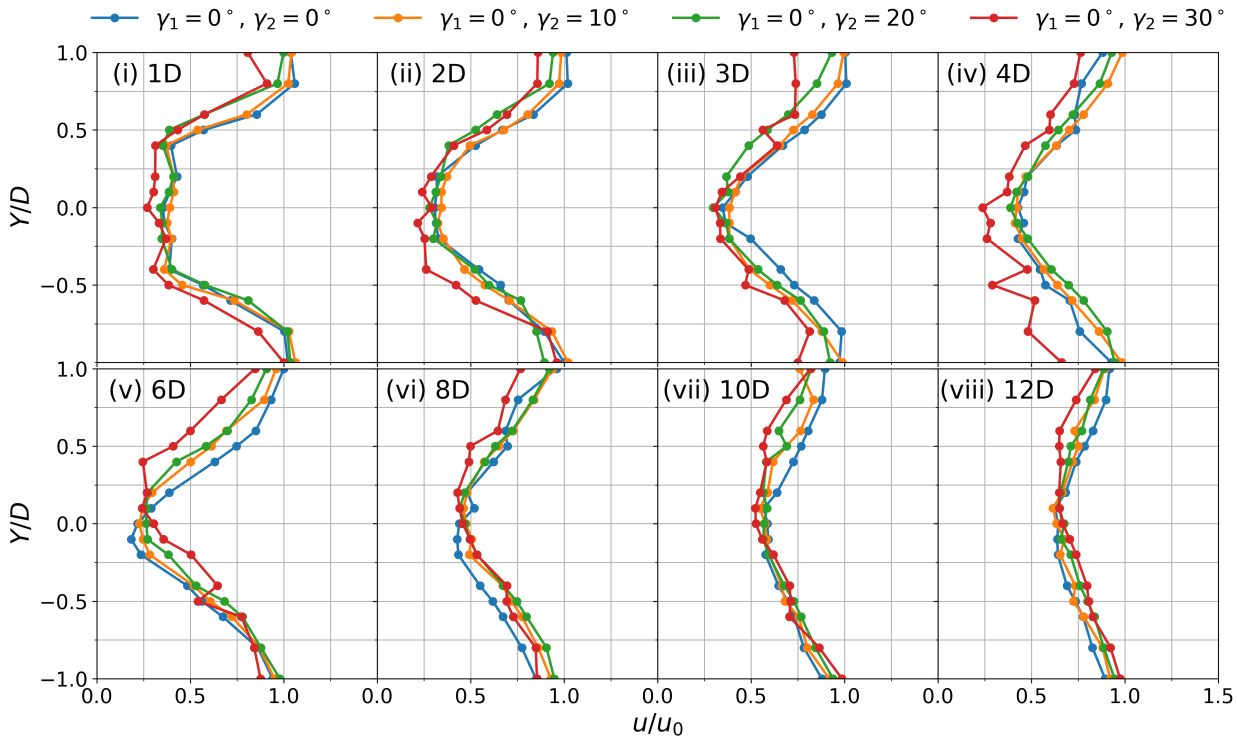

(**a**) Yawing the downstream turbine.

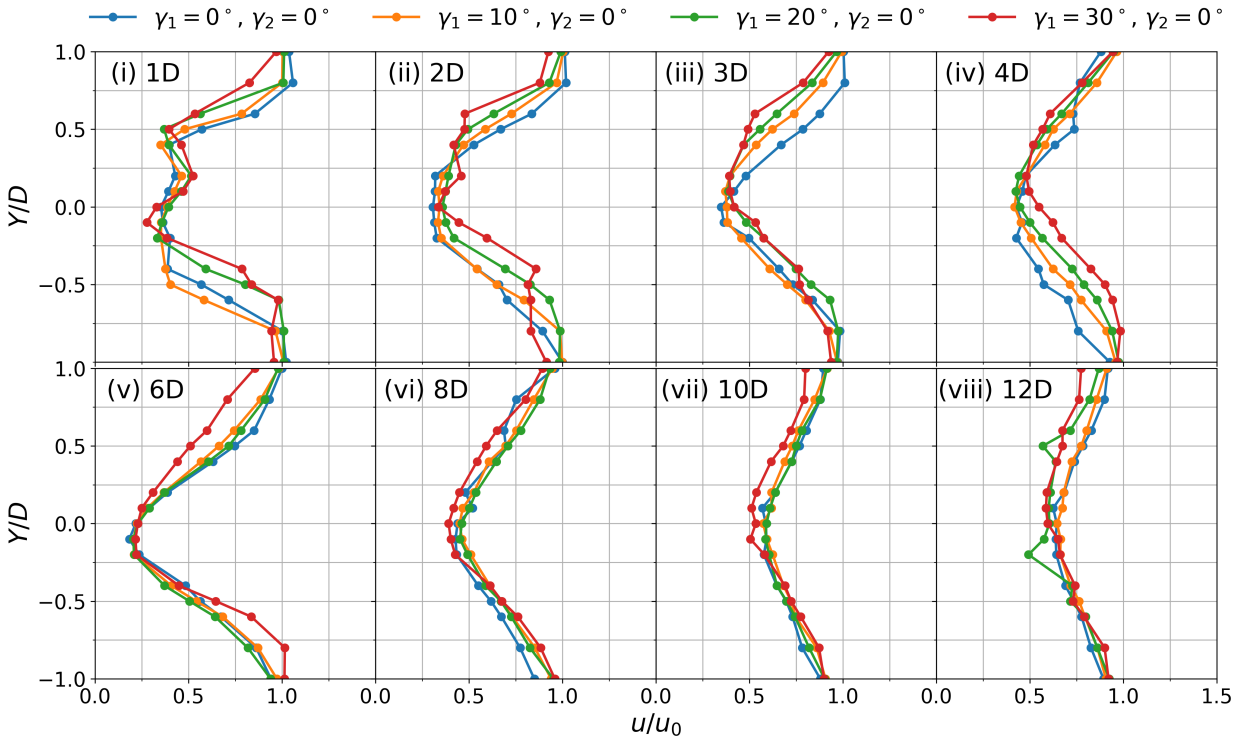

(**b**) Yawing the upstream turbine.

Figure 7. Normalised velocity distribution for the four cases considered in Scenario 2 at eight downstream cross-sections. The separation distance between the profiles and the turbine are (i) 1D, (ii) 2D, (iii) 3D, (iv) 4D, (v) 6D, (vi) 8D, (vii) 10D, and (viii) 12D, respectively.

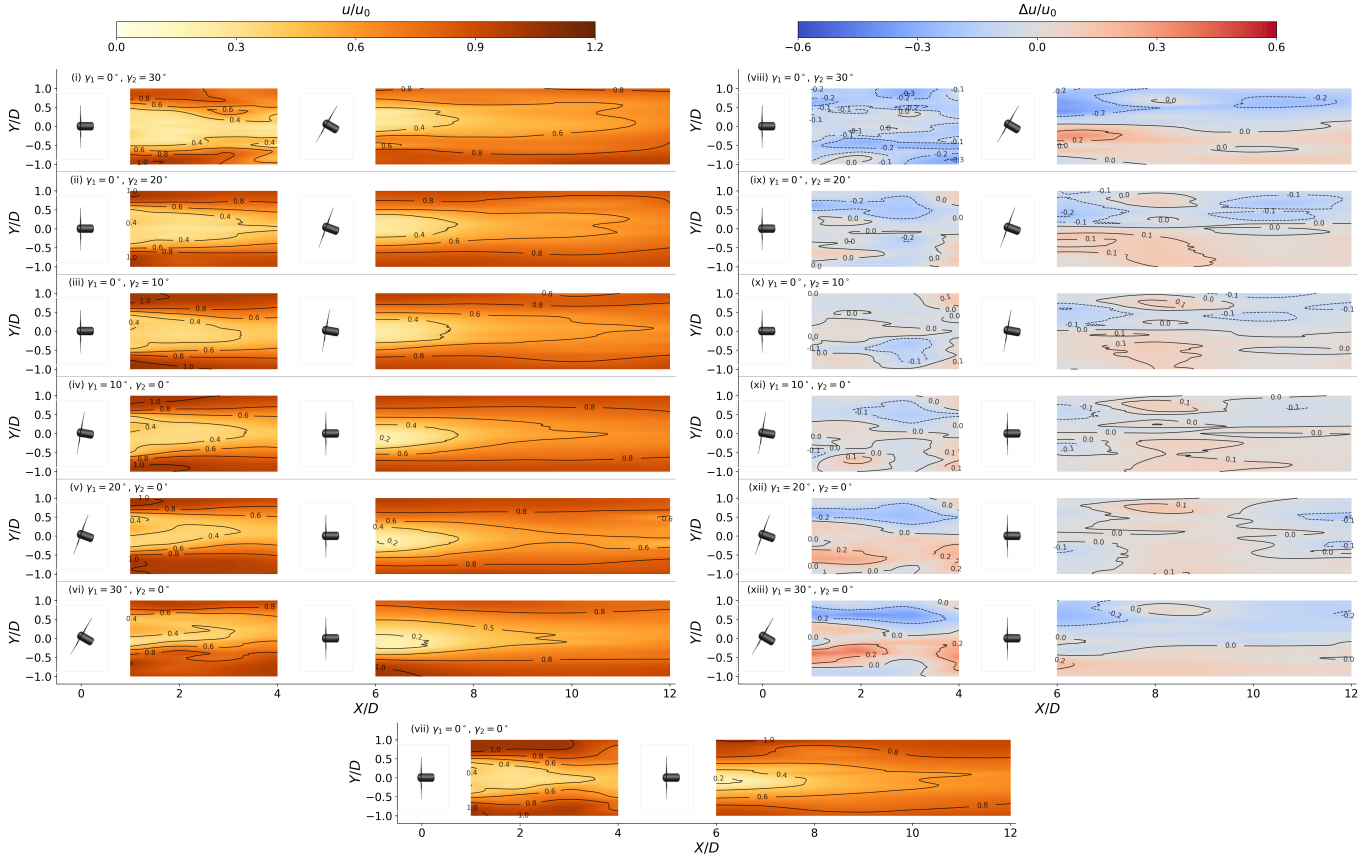

Figure 8. Normalised turbine wake velocity distributions for the cases of Scenario 2 and relative differences in normalised velocity between yawed and non-yawed turbine configurations: (i) $u/u_0 = u_{0°,10°}/u_0$, (ii) $u/u_0 = u_{0°,20°}/u_0$, (iii) $u/u_0 = u_{0°,30°}/u_0$, (iv) $u/u_0 = u_{10°,0°}/u_0$, (v) $u/u_0 = u_{20°,0°}/u_0$, (vi) $u/u_0 = u_{30°,0°}/u_0$, (vii) $u/u_0 = u_{0°,0°}/u_0$, (viii) $\Delta u/u_0 = (u_{0°,10°} - u_{0°,0°})/u_0$, (ix) $\Delta u/u_0 = (u_{0°,20°} - u_{0°,0°})/u_0$, (x) $\Delta u/u_0 = (u_{0°,30°} - u_{0°,0°})/u_0$, (xi) $\Delta u/u_0 = (u_{10°,0°} - u_{0°,0°})/u_0$, (xii) $\Delta u/u_0 = (u_{20°,0°} - u_{0°,0°})/u_0$, and (xiii) $\Delta u/u_0 = (u_{30°,0°} - u_{0°,0°})/u_0$. The quoted distances are downstream of the upstream turbine in all cases.

The distribution of velocity difference $\Delta u/u_0$ between the $\gamma_1 = 0°$ and $\gamma_1 > 0°$ cases are shown in Figure 8(xi–xiii). Compared to the $\gamma_1 = \gamma_2 = 0°$ case, the velocity magnitude at the northern side was smaller, and the flow was faster at the southern side across both wakes due to $\gamma_1 > 0°$. The magnitude of $\Delta u/u_0$ was sensitive to γ_1 in the upstream wake area. At a yaw angle of $\gamma_1 = 10°$, the highest value of $\Delta u/u_0$ was around 0.1. As $\gamma_1 > 10°$, wake steering was more pronounced. The velocity difference increased when the upstream turbine was yawed by 30°, and the highest absolute value of $\Delta u/u_0$ was around 0.3. The downstream wake area velocity difference was small. The main difference was induced by the yawed upstream turbine, where the recovery rate was faster in the downstream wake. It can be seen that most areas of the downstream wake showed a positive value of $\Delta u/u_0$ compared to the $\gamma_1 = \gamma_2 = 0°$ case. This was due to the less effective energy extraction ability of a yawed turbine, which mitigated some of the flow disturbance. As such, for $\gamma_1 > 0°$, we observed faster flow in the downstream wake area than in the non-yawed case. Only for the $\gamma_1 = 30°$ case did the downstream wake display the apparent yawed wake characteristic of higher velocity at the southern side and lower velocity at the northern side; the highest absolute values of $\Delta u/u_0$ for both sides reached 0.2.

3.3. Turbulence Intensity Distribution

3.3.1. Scenario 1: Single Turbine

Figure 9 shows the distribution of the streamwise turbulence intensity TI_x and relative plots of ΔTI_x between the $\gamma = 0°$ and $\gamma > 0°$ cases of Scenario 1.

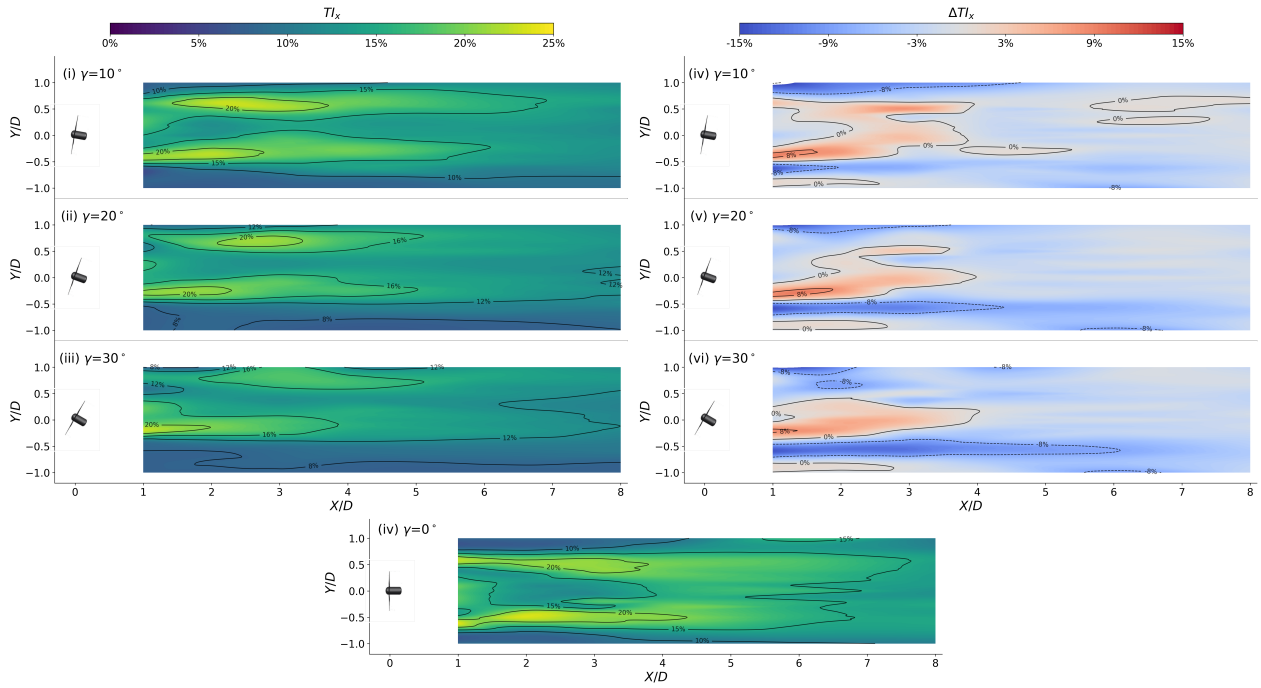

Figure 9. Streamwise turbulence intensity (left) and relative differences (right) between yawed and non-yawed cases of Scenario 1. (i) $TI_{x,\gamma=10°}$, (ii) $TI_{x,\gamma=20°}$, (iii) $TI_{x,\gamma=30°}$, (iv) $TI_{x,\gamma=0°}$, (v) $\Delta TI_x = TI_{x,\gamma=10°} - TI_{x,\gamma=0°}$, (vi) $\Delta TI_x = TI_{x,\gamma=20°} - TI_{x,\gamma=0°}$, and (vii) $\Delta TI_x = TI_{x,\gamma=30°} - TI_{x,\gamma=0°}$. The quoted distances are downstream of the upstream turbine in all cases.

As shown in Figure 9(i–iii), for $\gamma > 0°$, the rotor planes were not perpendicular to the inflow velocity, and thus, the TI_x values were not uniform over the cross-section. For $\gamma = 0°$ in Figure 9(iv), the highest TI_x value was around 20% in the near wake area at the vicinity of the blade tips. Lower TI_x values, of around 15%, were encountered in the central axis area. The bypass flow areas held the lowest value, which was less than 10%. This was because the rotor blade tips had the maximum line speed, and vortices were generated by flow separation at the blade tip edges. In the far-wake area, TI_x varied in a similar manner to the velocity deficit. With increasing distance downstream, TI_x gradually expanded in the transverse direction, and its value reduced to around 12% at an $8D$ downstream.

Figure 9(v–vii) subtract the streamwise turbulence intensity between yawed and non-yawed cases. In the near-wake area, TI_x decreased on the northern side, and the magnitude reduced as γ increased. At the same time, high TI_x values on the southern side moved towards the north, and as a result, there were both positive and negative ΔTI_x areas on the southern side. The central areas of TI_x in the yawed and non-yawed cases were almost the same around $1D$ and $2D$ as TI_x was mainly caused by the support structure. However, beyond $2D$, mixing effects increased the central area TI_x values with the wake steered towards the northern side. Therefore, higher TI_x values appeared in the central area.

The turbulence intensity difference in the far wake area was nearly negligible due to wake recovery. As an increasing yaw angle led to less disturbance of the flow and stronger mixing effects between the central and bypass flow, the ΔTI_x values between the $\gamma = 30°$ and non-yawed cases disappeared fastest.

3.3.2. Scenario 2: Yawing One of the Two Turbines

Figure 10 presents the turbulence intensity TI_x when only one of the turbines was yawed in Scenario 2. Figure 10(i–vii) show the normalised velocity TI_x distribution in Scenario 2, while Figure 10(viii–xiii) provide the normalised velocity difference ΔTI_x between the yawed and non-yawed turbine cases.

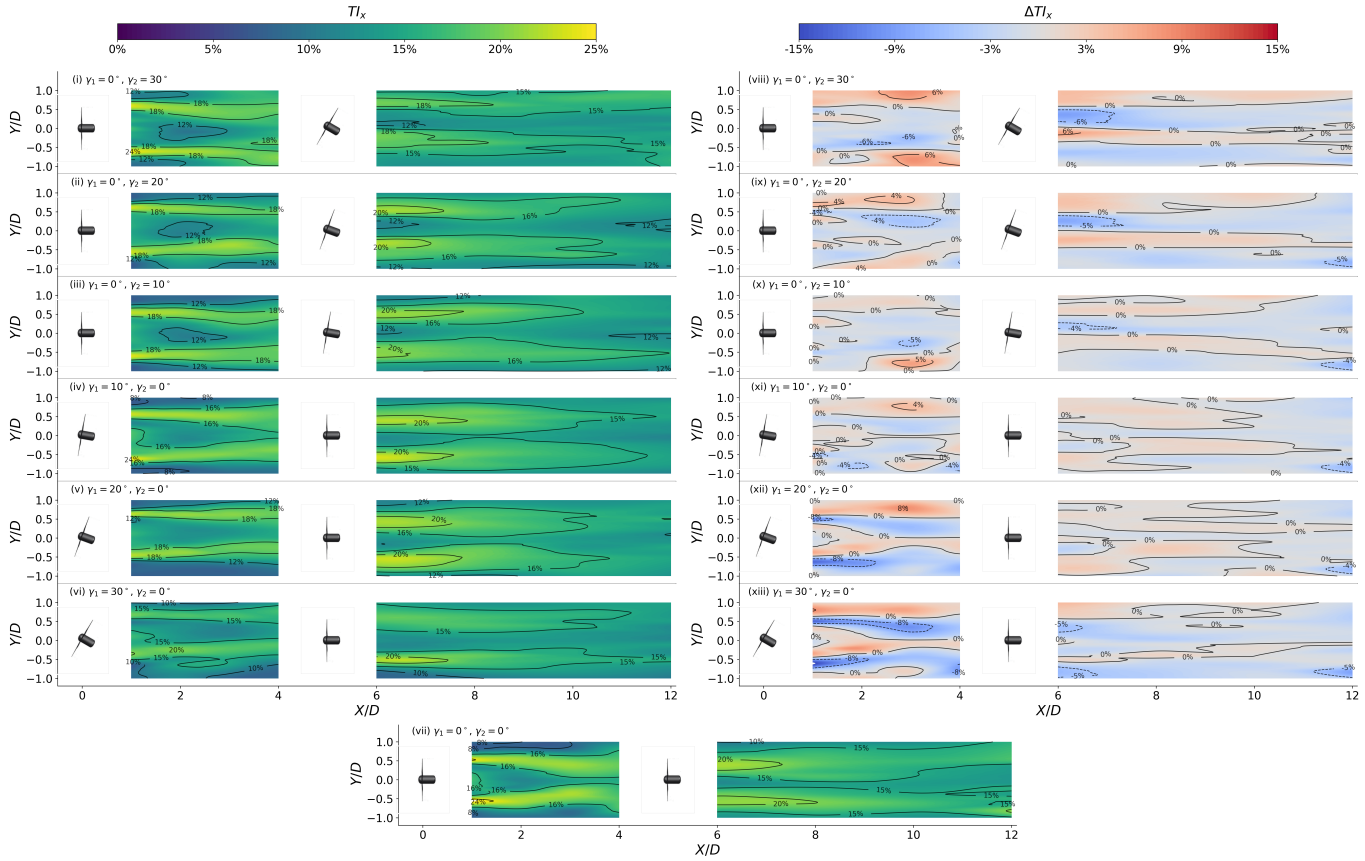

Figure 10. Distribution of streamwise turbulence intensity in the non-yawed case and relative differences between yawed and non-yawed cases for Scenario 2: (i) $TI_{x0^\circ,10^\circ}$, (ii) $TI_{x0^\circ,20^\circ}$, (iii) $TI_{x0^\circ,30^\circ}$, (iv) $TI_{x10^\circ,0^\circ}$, (v) $TI_{x20^\circ,0^\circ}$, (vi) $TI_{x30^\circ,0^\circ}$, (vii) $TI_{x0^\circ,0^\circ}$, (viii) $\Delta TI_x = TI_{x0^\circ,10^\circ} - TI_{x0^\circ,0^\circ}$, (ix) $\Delta TI_x = TI_{x0^\circ,20^\circ} - TI_{x0^\circ,0^\circ}$, (x) $\Delta TI_x = TI_{x0^\circ,30^\circ} - TI_{x0^\circ,0^\circ}$. (xi) $\Delta TI_x = TI_{x10^\circ,0^\circ} - TI_{x0^\circ,0^\circ}$, (xii) $\Delta TI_x = TI_{x20^\circ,0^\circ} - TI_{x0^\circ,0^\circ}$, and (xiii) $\Delta TI_x = TI_{x30^\circ,0^\circ} - TI_{x0^\circ,0^\circ}$. The quoted distances are downstream of the upstream turbine in all cases.

In the upstream wake area, when $\gamma_1 = 0^\circ$, the turbulence intensity in the central area was suppressed, and the highest turbulence intensity still appeared along the blade tip. For the $\gamma_1 = \gamma_2 = 0^\circ$ case, the TI_x value was 24% along the blade tip at $X/D = 1.0$, while the value in the central area was only 16%. The distribution of the turbulence intensity changed as $\gamma_2 > 0^\circ$. The TI_x values on the two sides increased compared to the non-yawed case, while the changes in the central area were negligible. The highest absolute value of ΔTI_x was above 6%, which appeared when $\gamma_2 = 30^\circ$. The significant turbulence intensity distribution difference between the $\gamma_2 = 0^\circ$ and $\gamma_2 > 0^\circ$ cases confirmed that the yawed downstream turbine can influence the flow upstream. As in Figure 10(viii–x), when $\gamma_1 > 0^\circ$, larger turbulence intensity values appeared at the northern side than for the baseline $\gamma_1 = \gamma_2 = 0^\circ$ case. With $\gamma_1 > 0^\circ$, the area with high-turbulence intensity moved north. The highest absolute value of ΔTI_x was found at 8%, in both the $\gamma_1 = 20^\circ$ and $\gamma_1 = 30^\circ$ cases, due to wake steering.

In the downstream wake area, the highest turbulence intensity decreased to 20%, dropping 4% compared to the value in the upstream wake area for the $\gamma_1 = \gamma_2 = 0^\circ$

case. This again can be explained as the incoming flow for the downstream turbine being decelerated by the upstream turbine. The ΔTI_x between the yawed and non-yawed cases diminished due to the decelerated flow driving the downstream turbine. The main turbulence intensity difference occurred at the edges of the wake when $\gamma_2 > 0°$, which gradually moved towards the northern side based on γ_2. When $\gamma_2 = 0°$, as in Figure 10(xi–xiii), the absolute value of ΔTI_x was less than 3% for most areas. The case where $\gamma_1 = 30°$ and $\gamma_2 = 0°$ was an exception, where ΔTI_x reached 5% at $6D$ downstream due to the severely steered front wake area caused by the upstream turbine.

3.4. Deflected Wake Centreline

The wake centreline can be used to examine the steered wake trajectory. We compared the wake centrelines in different scenarios to reveal the difference between three conditions: (a) a yawed turbine ($\gamma > 0°$) in isolation, which belongs to the cases of Scenario 1 where we denote the wake centreline as W; (b) a yawed turbine ($\gamma_1 > 0°$) with a non-yawed downstream turbine ($\gamma_2 = 0°$), which corresponds to cases of Scenario 2 when yawing the upstream turbine; we refer to the wake centreline in the upstream wake area as W_u; (c) a yawed turbine ($\gamma_2 > 0°$) with a non-yawed upstream turbine ($\gamma_1 = 0°$), which corresponds to the Scenario 2 cases when yawing the downstream turbine; we refer to the wake centreline in the downstream wake area as W_d. These centerlines are further defined in Figure 11. As all turbines yawed clockwise, the turbine wake steered toward the northern side of the domain, so we concentrated on this section of the domain.

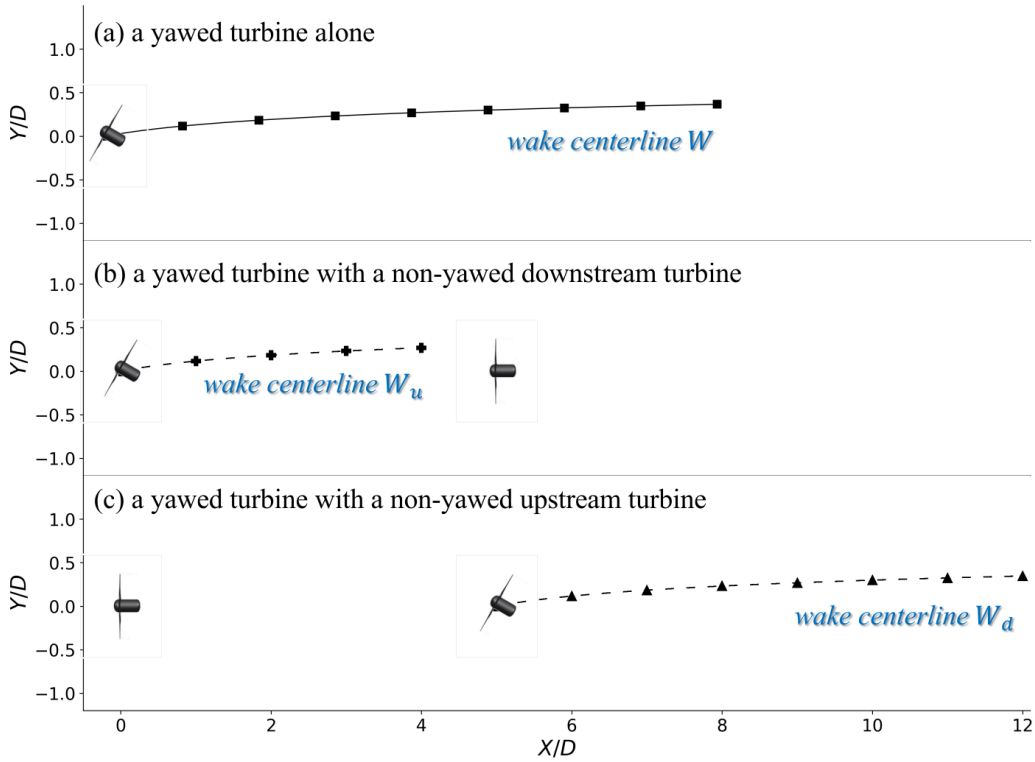

Figure 11. The definition of three types of wake centerlines for yawed turbines.

In Figure 12a, the baseline $\gamma = 0$ case is presented. The wake centerlines exhibited minor fluctuations along the $Y = 0D$ axis, which we attribute to the non-idealised physical experimental flow conditions. However, we saw that the wake centreline was not deflected in the absence of a discernible yaw angle. For a yaw angle of 10° (Figure 12b), the maximum spanwise shift of W was observed at $0.11D$. The deflection of W_u and W_d was similar in this case: the spanwise maximum shifts were both $\approx 0.05D$. This value is much smaller compared to the equivalent of W. In Figure 12c,d, it is noted that, while W remained the most deflected, the deflection of W_u became more apparent than W_d with an increase in

the yaw angle. This confirmed that, for the yawed wake, the deployment of a non-yawed turbine either upstream or downstream of a yawed turbine could limit the steering of the yawed turbine wake. Furthermore, an upstream non-yawed turbine would have a stronger effect on the yawed turbine wake deflection than a downstream non-yawed turbine would.

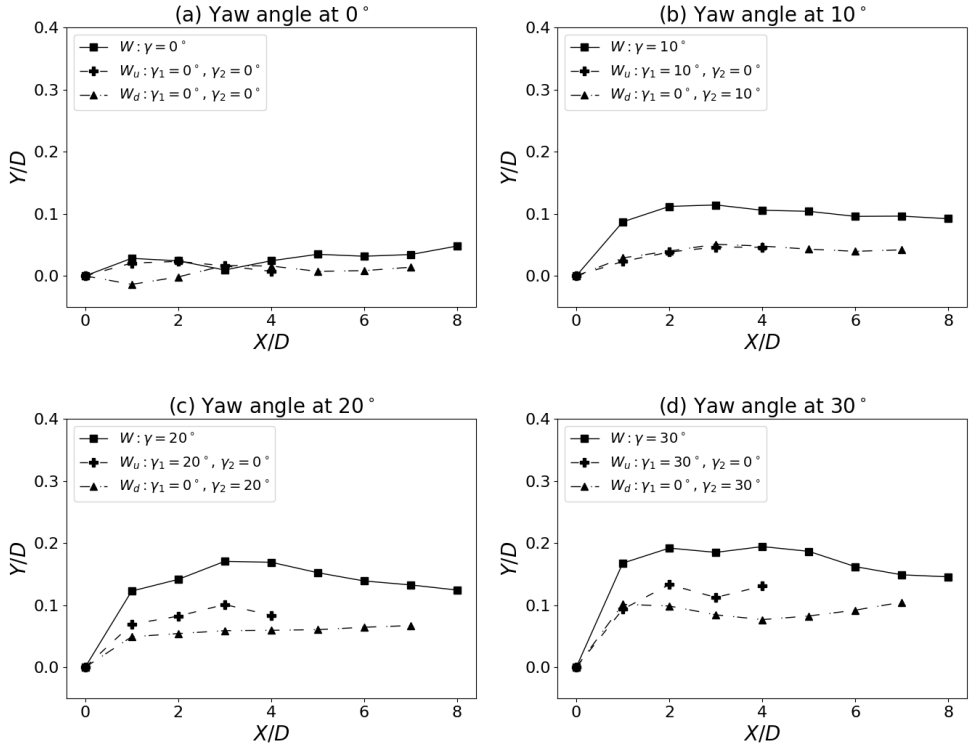

Figure 12. Wake centerlines under varying yaw angle cases. W: turbine wake centerline for Scenario 1; W_u: upstream turbine wake centerline for Scenario 2; W_d: downstream turbine wake centerline for Scenario 2. In all cases, the quoted distances for W and W_u are downstream of the upstream turbine, while the quoted distances for W_d are downstream of the downstream turbine.

As the γ varied from 10° to 30°, the deflection level for W, W_u, and W_d increased. For W, which had the most-significant wake centerline deflection, the spanwise maximum shift increased from $0.11D$ to $0.19D$. This demonstrated that the wake deflection level was proportional to the yaw angle.

Figure 13 shows the velocity deficit along each centerline. For the four yaw angle values considered, the differences in velocity deficit magnitudes at a $1D$ downstream between W and W_u are negligible. This is because the downstream turbine had an insignificant impact on the far-upstream area. However, they were both smaller than the velocity deficit along W_d, as the deficit value at the downstream wake was an accumulation result of the two turbines.

From $1D$ to $4D$, the velocity deficit along W_u remained at a high level regardless of the yaw angles. We attributed this to the significant disturbance from both turbines and the short distance available for wake recovery. From $4D$ to $7D$ downstream, when $\gamma \leq 20°$, the velocity deficits along W increased, firstly due to mixing with the slower flow behind the blade tip, then decreased because of further mixing with the fast flow outside the wake area. When $\gamma = 30°$, the velocity deficit behind the southern rotor edge tip was much smaller than the velocity deficit at the flume centre, as in Figure 6a. Therefore, mixing with the flow behind the blade tip appeared to contribute to the velocity recovery along the wake centreline, while the velocity deficit recovery was proportional to the downstream distance. Similarly, the velocities also recovered proportionally along W_d, as expected.

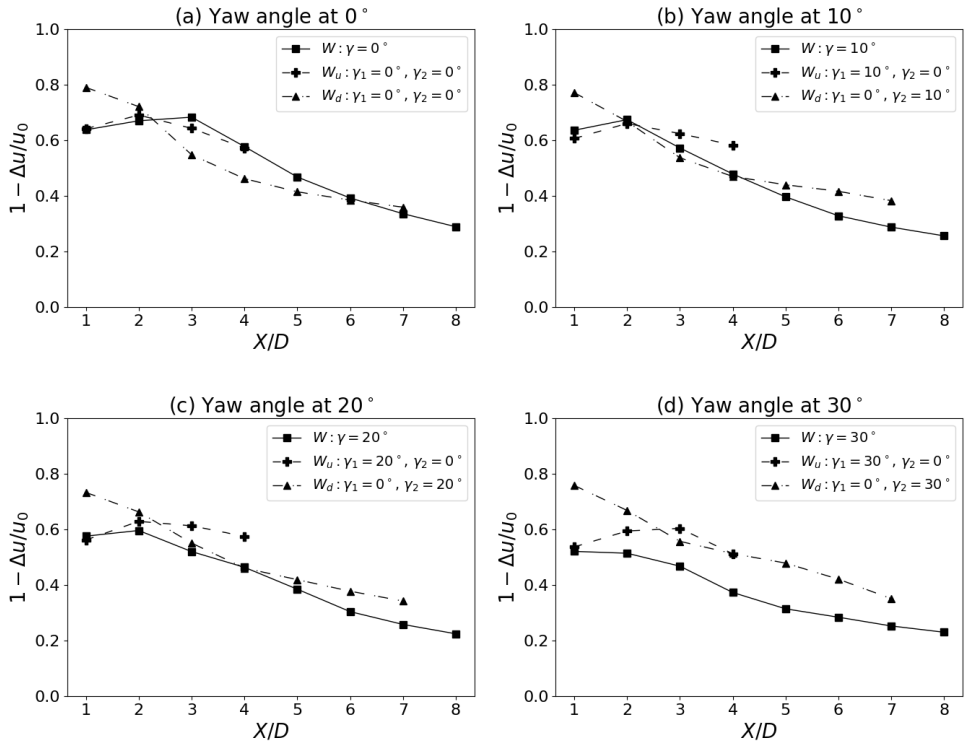

Figure 13. The velocity deficit along the wake centerlines under four different yaw angles. W: velocity deficit at wake centerlines in Scenario 1; W_u: velocity deficit at upstream wake centerlines in Scenario 2; W_d: velocity deficit at downstream wake centerlines in Scenario 2. In all cases, the quoted distances for W and W_u are downstream of the upstream turbine, while the quoted distances for W_d are downstream of the downstream turbine.

For each yaw angle, by comparing the velocity deficit at $7D$, it was found that the value of W was always smaller than the value of W_d. This demonstrated that the velocity had a higher recovery rate in the wake of a single-turbine setup than in the downstream wake of the two-turbine setup.

As the yaw angle increased from 0° to 30°, the velocity deficit at a $7D$ downstream reduced from 34% to 26% along W and from 38% to 35% along W_d. This confirmed that the wake velocities recovered faster with an increasing γ, which is in alignment with Adaramola and Krogstad [9].

4. Conclusions

Results from physical model experiments were presented on the investigation of the wake structure of yawed turbines in a recirculating current flume at Hohai University. Two different scenarios, which comprised 11 cases, were configured to test different yaw angle conditions. For each case, the thrust force of the turbine and the velocity values in the wake area at hub height were measured by an ATI-gamma six-axis force–torque sensor and a downward-facing Nortek Vectrino Profiler, respectively.

The force measurements showed that the thrust forces on the turbines decreased in the streamwise direction and increased in the spanwise direction when the yaw angle increased, as expected. From the comparison between the two cases in the two-turbine setup, it was found that, while a downstream non-yawed turbine had minimal effect on the yawed upstream turbine forces, an upstream non-yawed turbine could reduce the loads on a yawed downstream turbine by more than 50%.

For the wake trajectory evolution, results from the single-turbine cases showed that the wake was steered in a counterclockwise direction with clockwise turbine yawing as a result of the force balance on the rotor. Wake deflection increased, and the wake velocity recovered

faster as the yaw angle increased. For the two-turbine cases, it was noted that a non-yawed upstream turbine limited the performance of the yawed downstream turbine, but the latter could still steer the downstream wake. Interestingly, when an upstream turbine was yawed, which included a downstream turbine in its wake region, the intermediate velocity profiles between the devices evolved according to the observations for the single-turbine cases. On the other hand, the flow immediately downstream of the second non-yawed turbine was dominated by the second device.

Measurements of the turbulence intensity showed that the highest turbulence intensity occurred behind the blade tips. As the turbine rotated clockwise and the yaw angle increased, the turbulence intensity became asymmetric, with the higher values appearing on the north side.

The "Centre of Mass" method was used to determine the wake centrelines. The results showed that the deflection level of the wake centerline was closely linked to the yaw angle. Over the $7D$ considered for the velocity recovery, the velocity at the centerline achieved a higher recovery rate with a larger yaw angle. For each yaw angle, by comparing the centreline deflection of the yawed turbine wake from the three cases, (a) a single yawed turbine, (b) a yawed turbine with a non-yawed turbine upstream, and (c) a yawed turbine with a non-yawed turbine downstream, it was noted that, for the yawed wake, the deployment of a non-yawed turbine either upstream or downstream of a yawed turbine always limited the deflection of the yawed turbine wake. Similarly, for the velocity deficit at the wake centerline, the single yawed turbine case had the smallest velocity deficit at a $7D$ downstream for each yaw angle. Furthermore, by comparing Case (b) to (c), we found that an upstream non-yawed turbine would have a deeper effect on the yawed turbine wake deflection than a downstream non-yawed turbine would.

This study provided substantial data about yawed turbine wakes. Based on the results presented above, it was found that, although yawed turbines steered their wakes, the downstream turbine, especially if aligned with the upstream turbine, would still be affected. Therefore, a staggered layout, with respect to the dominant tidal flow directions, would likely still be a better choice than an aligned layout for the application of a yaw control wake steering strategy. In future work, we plan to use the results presented here to validate a yawed turbine model as implemented in 2D in the depth-averaged version of the Thetis ocean model [29,43]. The preliminary results obtained with this model indicated promising agreement for yaw angles below 20°, with further investigations planned based on the observed data collected herein. Furthermore, we intend to combine the yawed turbine simulation model with optimisation algorithms to investigate possible improvements when the ability to control the yaw angle is considered during the design of optimal turbine array layouts.

Author Contributions: Conceptualization, C.Z., J.Z. and M.D.; Methodology, J.Z. and M.D.; Validation, C.Z.; Formal analysis, C.Z., A.A., Y.Z. and S.K.; Investigation, C.Z.; Resources, J.Z.; Writing—Original Draft, C.Z.and A.A.; Writing—review & editing, C.Z., J.Z., A.A., S.K. and M.D.; Supervision, J.Z. and M.D.; Funding Acquisition, C.Z., J.Z. and M.D. All authors have read and agreed to the published version of the manuscript.

Funding: This research was funded by China Scholarship Council (grant number 201906710084), the Fundamental Research Funds for the Central Universities (grant number B210203022), the National Natural Science Foundation of China (grant number 51879098), the Key Project of NSFC-Shangdong Joint Research Funding POW3C (grant number U1906230) and the U.K.'s Engineering and Physical Sciences Research Council (grant number EP/R029423/1 and EP/R007470/1).

Data Availability Statement: Data available on request due to restrictions.

Acknowledgments: The authors are grateful for the sponsorship from the China Scholarship Council (Project No. 201906710084), the Fundamental Research Funds for the Central Universities (Project B210203022), the National Natural Science Foundation of China (Project 51879098), and the Key Project of NSFC-Shangdong Joint Research Funding POW3C (U1906230). The authors also acknowl-

edge the support of the U.K.'s Engineering and Physical Sciences Research Council under Projects EP/R029423/1 and EP/R007470/1.

Conflicts of Interest: The authors declare no conflict of interest.

References

1. Melikoglu, M. Current status and future of ocean energy sources: A global review. *Ocean Eng.* **2018**, *148*, 563–573. [CrossRef]
2. Neill, S.P.; Haas, K.A.; Thiébot, J.; Yang, Z. A review of tidal energy–Resource, feedbacks, and environmental interactions. *J. Renew. Sustain. Energy* **2021**, *13*, 062702. [CrossRef]
3. Coles, D.; Angeloudis, A.; Greaves, D.; Hastie, G.; Lewis, M.; Mackie, L.; McNaughton, J.; Miles, J.; Neill, S.; Piggott, M.; et al. A review of the UK and British Channel Islands practical tidal stream energy resource. *Proc. R. Soc. A* **2021**, *477*, 20210469. [CrossRef] [PubMed]
4. Piggott, M.D.; Kramer, S.C.; Funke, S.W.; Culley, D.M.; Angeloudis, A. Optimization of Marine Renewable Energy Systems. In *Comprehensive Renewable Energy (Second Edition)*, 2nd ed.; Letcher, T.M., Ed.; Elsevier: Oxford, UK, 2022; pp. 176–220. . [CrossRef]
5. Frost, C.; Morris, C.E.; Mason-Jones, A.; O'Doherty, D.M.; O'Doherty, T. The effect of tidal flow directionality on tidal turbine performance characteristics. *Renew. Energy* **2015**, *78*, 609–620. [CrossRef]
6. Frost, C.H.; Evans, P.S.; Harrold, M.J.; Mason-Jones, A.; O'Doherty, T.; O'Doherty, D.M. The impact of axial flow misalignment on a tidal turbine. *Renew. Energy* **2017**, *113*, 1333–1344. [CrossRef]
7. Modali, P.K.; Vinod, A.; Banerjee, A. Towards a better understanding of yawed turbine wake for efficient wake steering in tidal arrays. *Renew. Energy* **2021**, *177*, 482–494. [CrossRef]
8. Burton, T.; Jenkins, N.; Sharpe, D.; Bossanyi, E. *Wind Energy Handbook*; John Wiley & Sons: Hoboken, NJ, USA, 2011.
9. Adaramola, M.; Krogstad, P.Å. Experimental investigation of wake effects on wind turbine performance. *Renew. Energy* **2011**, *36*, 2078–2086. [CrossRef]
10. Howland, M.F.; Lele, S.K.; Dabiri, J.O. Wind farm power optimization through wake steering. *Proc. Natl. Acad. Sci. USA* **2019**, *116*, 14495–14500. [CrossRef]
11. Bastankhah, M.; Porté-Agel, F. Experimental and theoretical study of wind turbine wakes in yawed conditions. *J. Fluid Mech.* **2016**, *806*, 506–541. [CrossRef]
12. Gao, Z.; Li, Y.; Wang, T.; Shen, W.; Zheng, X.; Pröbsting, S.; Li, D.; Li, R. Modelling the nacelle wake of a horizontal-axis wind turbine under different yaw conditions. *Renew. Energy* **2021**, *172*, 263–275. [CrossRef]
13. Dijk, M.V.; Wingerden, J.V.; Ashuri, T.; Li, Y. Wind farm multi-objective wake redirection for optimizing power production and loads. *Energy* **2017**, *121*, 561–569. [CrossRef]
14. Bartl, J.; Mühle, F.; Stran, L. Wind tunnel study on power output and yaw moments for two yaw-controlled model wind turbines. *Wind Energy Sci.* **2018**, *3*, 489–502. [CrossRef]
15. Zong, H.; Porté-Agel, F. Experimental investigation and analytical modelling of active yaw control for wind farm power optimization. *Renew. Energy* **2021**, *170*, 1228–1244. [CrossRef]
16. Bastankhah, M.; Porté-Agel, F. Wind farm power optimization via yaw angle control: A wind tunnel study. *J. Renew. Sustain. Energy* **2019**, *11*, 023301. [CrossRef]
17. Bahaj, A.; Molland, A.; Chaplin, J.; Batten, W. Power and thrust measurements of marine current turbines under various hydrodynamic flow conditions in a cavitation tunnel and a towing tank. *Renew. Energy* **2007**, *32*, 407–426. [CrossRef]
18. Galloway, P.W.; Myers, L.E.; Bahaj, A. Quantifying wave and yaw effects on a scale tidal stream turbine. *Renew. Energy* **2014**, *63*, 297–307. [CrossRef]
19. Ke, S.; Wen-Quan, W.; Yan, Y. The hydrodynamic performance of a tidal-stream turbine in shear flow. *Ocean Eng.* **2020**, *199*, 107035. [CrossRef]
20. O'Rourke, F.; Boyle, F.; Reynolds, A.; Kennedy, D.M. Hydrodynamic performance prediction of a tidal current turbine operating in non-uniform inflow conditions. *Energy* **2015**, *93*, 2483–2496. [CrossRef]
21. Baratchi, F.; Jeans, T.L.; Gerber, A.G. Actuator line simulation of a tidal turbine in straight and yawed flows - ScienceDirect. *Int. J. Mar. Energy* **2017**, *19*, 235–255. [CrossRef]
22. Wang, S.J.; Jiang, X.Y.; Yuan, P.; Xian-Cai, S.I.; Xiao-Li, Y.U. Performance and Wake Characteristics Analysis for Tidal Turbine with Yaw Angle. *Period. Ocean. Univ. China* **2019**, *49*, 122–128.
23. Borg, M.G.; Xiao, Q.; Allsop, S.; Incecik, A.; Peyrard, C. A numerical performance analysis of a ducted, high-solidity tidal turbine in yawed flow conditions. *Renew. Energy* **2022**, *193*, 179–194. [CrossRef]
24. Zhang, C.; Kramer, S.; Angeloudis, A.; Zhang, J.; Lin, X.; Piggott, M.D. Improving tidal turbine array performance through the optimisation of layout and yaw angles. In Proceedings of the 14th European Wave and Tidal Energy Conference, EWTEC, Plymouth, UK, 5–9 September 2021; pp. 1–7.
25. Jordan, C.; Dundovic, D.; Fragkou, A.K.; Deskos, G.; Coles, D.S.; Piggott, M.D.; Angeloudis, A. Combining shallow-water and analytical wake models for tidal array micro-siting. *J. Ocean. Eng. Mar. Energy* **2022**, *8*, 193–215. [CrossRef]
26. Zhou, Y.; Wang, G.; Lin, X.; Zhang, J. Experimental Study of Wake Flow around a Twin-rotor Tidal Stream Turbine. In Proceedings of the The 31st International Ocean and Polar Engineering Conference, Rhodes, Greece, 20–25 June 2021; OnePetro: Richardson, TX, USA, 2021.

27. Wang, G. Study on Wake Distribution and Force Characteristics of Tidal Current Energy Array. Master's Thesis, Hohai University, Nanjing, China, 2021.
28. Coles, D.; Blunden, L.; Bahaj, A. The energy yield potential of a large tidal stream turbine array in the Alderney Race. *Philos. Trans. R. Soc. A* **2020**, *378*, 20190502. [CrossRef] [PubMed]
29. Zhang, J.; Zhou, Y.; Lin, X.; Wang, G.; Guo, Y.; Chen, H. Experimental investigation on wake and thrust characteristics of a twin-rotor horizontal axis tidal stream turbine. *Renew. Energy* **2022**, *195*, 701–715. [CrossRef]
30. Zang, W.; Zheng, Y.; Zhang, Y.; Zhang, J.; Fernandez-Rodriguez, E. Experiments on the mean and integral characteristics of tidal turbine wake in the linear waves propagating with the current. *Ocean Eng.* **2019**, *173*, 1–11. . [CrossRef]
31. Chen, Y.; Lin, B.; Lin, J.; Wang, S. Experimental study of wake structure behind a horizontal axis tidal stream turbine. *Appl. Energy* **2017**, *196*, 82–96. . [CrossRef]
32. Kang, S.; Kim, Y.; Lee, J.; Khosronejad, A.; Yang, X. Wake interactions of two horizontal axis tidal turbines in tandem. *Ocean Eng.* **2022**, *254*, 111331. [CrossRef]
33. Zhang, Y.; Zhang, J.; Lin, X.; Wang, R.; Zhang, C.; Zhao, J. Experimental investigation into downstream field of a horizontal axis tidal stream turbine supported by a mono pile. *Appl. Ocean Res.* **2020**, *101*, 102257. [CrossRef]
34. Zhang, J.; Lin, X.; Wang, R.; Guo, Y.; Zhang, C.; Zhang, Y. Flow structures in wake of a pile-supported horizontal axis tidal stream turbine. *Renew. Energy* **2020**, *147*, 2321–2334. [CrossRef]
35. Fleming, P.A.; Gebraad, P.M.; Lee, S.; van Wingerden, J.W.; Johnson, K.; Churchfield, M.; Michalakes, J.; Spalart, P.; Moriarty, P. Evaluating techniques for redirecting turbine wakes using SOWFA. *Renew. Energy* **2014**, *70*, 211–218. [CrossRef]
36. Modali, P.K. On Performance and Wake Characteristics of a Tidal Turbine under Yaw. PhD Thesis, Lehigh University, Bethlehem, PA, USA, 2016. [CrossRef]
37. Howland, M.F.; Bossuyt, J.; Martínez-Tossas, L.A.; Meyers, J.; Meneveau, C. Wake structure in actuator disk models of wind turbines in yaw under uniform inflow conditions. *J. Renew. Sustain. Energy* **2016**, *8*, 043301. [CrossRef]
38. Jiménez, Á.; Crespo, A.; Migoya, E. Application of a LES technique to characterize the wake deflection of a wind turbine in yaw. *Wind Energy* **2010**, *13*, 559–572. [CrossRef]
39. Luo, L.; Srivastava, N.; Ramaprabhu, P. A study of intensified wake deflection by multiple yawed turbines based on large eddy simulations. In Proceedings of the 33rd Wind Energy Symposium, Kissimmee, FL, USA, 5–9 January 2015; p. 0220.
40. Trujillo, J.J.; Bingöl, F.; Larsen, G.C.; Mann, J.; Kühn, M. Light detection and ranging measurements of wake dynamics. Part II: two-dimensional scanning. *Wind Energy* **2011**, *14*, 61–75. [CrossRef]
41. Fleming, P.A.; Gebraad, P.M.; Churchfield, M.J.; van Wingerden, J.W.; Scholbrock, A.K.; Moriarty, P.J. Using particle filters to track wind turbine wakes for improved wind plant controls. In Proceedings of the 2014 American Control Conference, Portland, OR, USA, 4–6 June 2014; IEEE: Piscataway, NJ, USA, 2014; pp. 3734–3741.
42. Modali, P.; Kolekar, N.S.; Banerjee, A. Performance and wake characteristics of a tidal turbine under yaw. *Int. Mar. Energy J.* **2018**, *1*, 41–50. [CrossRef]
43. Kärnä, T.; Kramer, S.C.; Mitchell, L.; Ham, D.A.; Piggott, M.D.; Baptista, A.M. Thetis coastal ocean model: Discontinuous Galerkin discretization for the three-dimensional hydrostatic equations. *Geosci. Model Dev.* **2018**, *11*, 4359–4382. [CrossRef]